Thrust vectoring effects of a transverse gas injection into a supersonic cross-flow of an axisymmetric C-D nozzle

V. Zmijanovic[1], V. Lago, L. Leger, E. Depussay [1], S. Palerm, J. Oswald[2], M.Sellam and A. Chpoun[3]
[1] C.N.R.S. -Institute ICARE, 1C Avenue de la Recherche Scientifique, 45071 Orléans cedex 2, France
[2] C.N.E.S. -Direction de lanceurs, Rond point de l'Espace, 91023 Courcouronnes-Evry cedex, France
[3] L.M.E.E., Université d'Evry Val d'Essonne, 40 rue du Pelvoux, 91020 Evry cedex, France

Abstract
The transverse gas injections into the main, supersonic flow of an axisymmetric C-D nozzle are investigated for the fluid thrust vectoring possibilities as the segment part of the CNES "Perseus" project. Two C-D conical type nozzles with different position of the secondary sonic injection port are chosen as the test-models in experimental and numerical study of this investigation. Analytical approach revealed parameters which influence the fluidic thrust vectoring efficiency, these aspects are further numerically explored and results-data is compared with experiments of the same test-case. It is found that with moderate secondary to primary mass-flow ratios from 5%, pertinent vector side force is obtained.

1. Introduction

The supersonic cross-flow jet interactions of a sonic injection into the oncoming supersonic main stream are the issue in numerous aerospace engineering applications ranging from the supersonic scramjet combustors and hypersonic vehicle reaction control jets to the fluidic thrust vectoring systems. The perspectives of fluidic thrust vector control (FTV) via transverse gas injection are of the special interest to the small space vehicles and systems. The elimination of the heavy and complex actuators of conventional mechanic TVC largely reduces the mass of the system and simplify design with utilisation of only fast-opening valves. The fast dynamic response of the fluidic thrust-vectoring system (~900Hz) [16] comparing to conventional of ~30Hz [12]and smaller loss in the thrust specific impulse, additionally emphasize FTV as an attractive alternative in thrust vectoring of a rocket engine. These characteristics are inline with the needs of small launching vehicles, satellite's attitude control and docking modules. The CNES "Perseus" project is devoted to the development of the small "micro" launcher systems among which optimal solution should be found for cost-effective launch of small "micro and nano" satellites. The promising large reduction in mass and size, simplicity, fast response and possible effectiveness are highly beneficial to the vector control system of the small launchers intended by the CNES "Perseus".

There are a number of different modes of fluidic thrust vectoring as the skewing of the throat sonic line or counter and co-flow control at the nozzle exit. The secondary gas injection thrust-vector control (SITVC) or also known as shock vector control (SVC) represents direct and straightforward type of the FTV at which the gas is injected at the divergent section of the C-D nozzle in order to separate the flow from the nozzle wall, create strong shock and deviate the main jet direction. The secondary gas is injected via the tubing and fast valves directly from the combustion chamber to the divergent section. In order not too largely affect performance of regular rocket engine operation-cycle, secondary injection of mass-flow ratio m_j/m_i ~5% is intended. Investigation experimental and numerical results of the C-D conical type nozzles are elaborated and presented in this work with addition of TIC nozzle numerical simulation result-data.

Nomenclature

SITVC	-	Secondary injection thrust vector control
SVC	-	Shock vector control
TVC	-	Thrust vector control
FTV	-	Fluidic thrust vectoring
TIC	-	Truncated ideal contour
CFD	-	Computational fluid dynamics
CPS	-	Code pour la propulsion spatiale

PUV	-	Primary upstream vortex
SUV	-	Secondary upstream vortex
PDV	-	Primary downstream vortex
SDV	-	Secondary downstream vortex
NPR	-	p_c/p_a Nozzle pressure ratio
SPR	-	p_j/p_c Secondary pressure ratio
3D	-	three-dimensional
2D	-	two-dimensional
M	-	Mach number
p_c	-	Chamber stagnation pressure
p_j	-	Second injection pressure
p_a	-	Ambient pressure
m_i	-	primary mass-flow-rate
m_j	-	secondary mass-flow-rate
f_m	-	m_j/m_i mass-flow ratio
x	-	Nozzle axis with coordinate beginning at the nozzle throat
x_t	-	Divergent length of the nozzle
x_j	-	x-coordinate of the secondary injection port
x/x_i	-	Dimensionless x coordinate
h	-	Injectant Mach disk height (distance from the nozzle wall)
δ	-	Pitch thrust-vector deflection angle
φ	-	Circular arc central angle
θ	-	Injection angle with respect to nozzle axis
γ	-	C_p/C_v heat capacity ratio
y+	-	$(u \cdot y)/\nu$ dimensionless wall distance
F_a	-	Axial thrust force
F_w	-	Force on the nozzle wall
F_j	-	Second injection reactive force (dynalpy flux)
$F_{x,y,z}$	-	force components in x,y and z direction
I_{sp}	-	specific impulse

1.2 Analytical approach and description

The strong shocks generated by the secondary injection at divergent (supersonic) portion of the nozzle are mainly responsible for diverting the nozzle jet. This resulting flowfield is characterized with the complex flow structures featuring the three-dimensional vortex and shock regions with the strong adverse pressure gradients, boundary-layer separation, shock generation and their interaction, vortex shedding and wakes, detached flow and mixing shear layers.

The secondary injectant in the flow is acting as an obstacle and source of main jet momentum change. The upstream separation distance is in general determined by the flow nature at the boundary-layer (laminar or turbulent) and by the penetration height of the injectant, as reported by Spaid et al.[3] In the basic case Figure 1., the turbulent boundary-layer of the main flow is detached upstream of the injection port due to an adverse pressure gradient with the generation of the separation shock. Further downstream, this weaker separation shock is interacting with the strong bow shock which is formed in front of the injection plume as a consequence of the main jet obstruction. This interaction and the shock structure are giving steeper gradient to the main flow deflection while between the shock region and the wall recirculation shock-bubble is formed. The structure between the wall, shock region and the injectant plume, Figure 1, involves the counter-rotating vortex pair, commonly known as the primary upstream vortex (PUV) which develops along the wall boundary and smaller counter-rotating secondary upstream vortex (SUV) near the injectant plume. The separation shock formed along the displaced boundary-layer by these vortices and sonic surface in between them are essentially deviate the incoming flow. The separation shock is then interacting with the strong bow shock which is formed in the main flow as a consequence of obstruction by the transverse injectant. Sonically injected gas is under-expanded, thus, it is expanding in the main flow through the Parndtl-Meyer fan and is recompressed by the barrel shock formation with the Mach disk at the end of this process.

On the other side, diverted main flow is turning the transverse jet parallel towards the wall where on the downstream side after injection port recompression and reattachment shocks are present and followed by the primary and secondary downstream wake vortices (PDV and SDV).

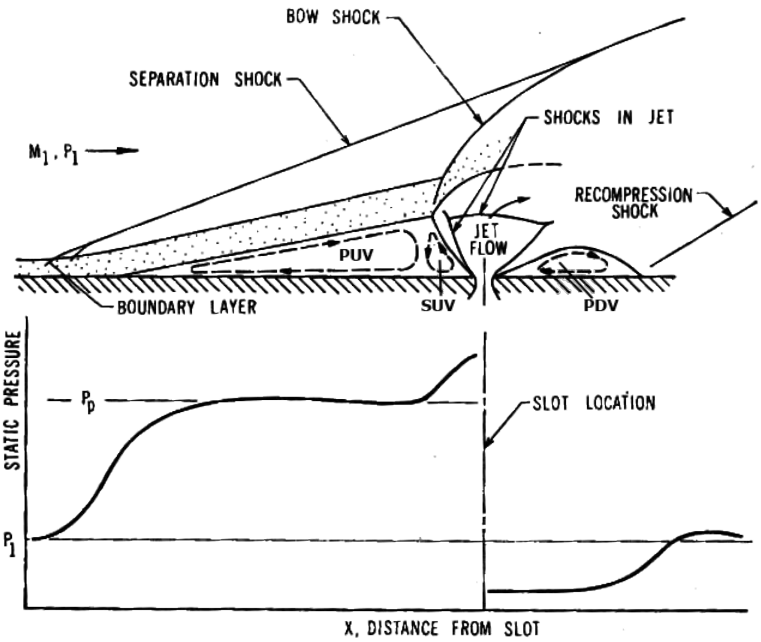

Figure 1: 2D flowfield and pressure distribution of transverse slot gas injection by Spaid and Zukoski [3]

Investigations on the jet cross-flow type of interactions have emerged since the early ‘60s. The first works have been devoted to the fundamental, 2D, case of normal slot sonic injection at the flat plate into the supersonic stream, as referenced Spaid et al [3] Avduevski et al.[7]. The goal was to analytically shape the problem and occurring processes that happen, primarily, the boundary-layer detachment, height of the injectant penetration, shock waves generation and their propagation. The Zukoski [4] found that transverse injection is obstructing the main supersonic stream in a quite similar manner as the forward-faced step in supersonic flow. This is further improved with Spaid, Zukoski [3] blunt-body analytical model where forward face of the blunt body has a curvature with radius half of the injectant height, Figure 2.

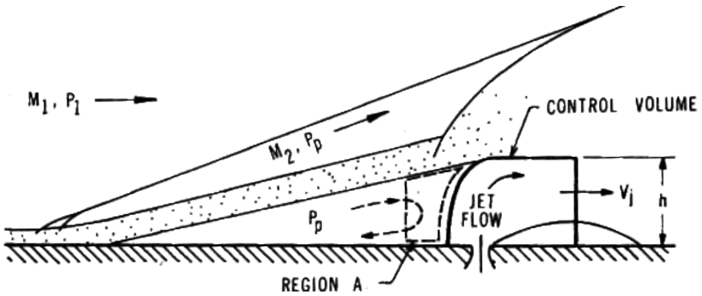

Figure 2: Blunt-body model of transverse injection into supersonic stream by Spaid et al. [3]

The necessary assumptions in all analytical models may generate errors in some domains and cause the model limited in some range of observation. The blunt-body model showed well in moderate mass-flow ratios and smaller pressure ratios which is relatively close to the range in which thrust shock vector control is investigated. The equation 1 solved for h and combined with separation criterion using the relation of plateau pressure and one of the control volume, leads to the position of the separation point, also reported by Maarouf et al. [11].

$$\frac{\pi}{4} q_0 C_{ps} h^2 - \frac{2}{3} q_0 C_{ps} y_j f h = 2 c_d b y_j f \gamma p_j \left(\frac{2}{\gamma+1}\right)^{\frac{1}{\gamma-1}} \left[\frac{1}{\gamma^2-1}\left(1-\left(\frac{p_s}{p_j}\right)^{\frac{\gamma-1}{\gamma}}\right)\right]^{\frac{1}{2}} \quad \textbf{(1)}$$

From the beginning of the ‘90s computational fluid dynamics (CFD) is extensively used in supersonic cross-flow jet interactions research. The model and experiments performed by Spaid and Zukoski [3,4] are referential for the code validation in number of works based on CFD methods as Erdem et al. [13]. Together with supersonic turbulent boundary layer findings [14] the analytic models has been further developed and occurring effects better resolved.

The circular sonic injection at the flat plate, on other hand, is characterized with the more complex three-dimensional (3D) flow structure. The separation upstream vortices PUV and SUV are in this case forming spanwise 3D horseshoe shaped vortex regions. The bow shock has a 3D flow nature as well spreading spanwise around and above the secondary injection plume. The simplified scheme of circular injection is reported by Santiago et al. [2], and depicted on the Figure 3. The circular sonic injection is parametrically analyzed by Shetz and Billig [6] and also by the early researchers on the topic of fluidic thrust vectoring of axisymmetric nozzles as Nielson et al. [1] and Guhse [5]. From the parametric point of view aspects that should be paid attention to in FTV investigation may be listed as: 1. Point of injection, 2. Secondary gas flow rate determined (a. the injection port area A_j, b. the secondary and primary stagnation pressure SPR and NPR), 3. Geometrical shape of injection port, 4. Angle of injection and 5. Primary and secondary gas properties.

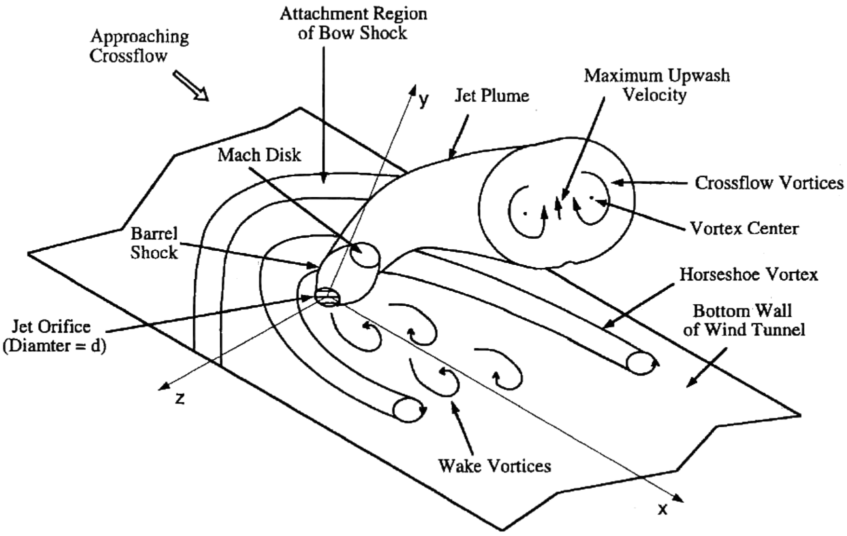

Figure 3: Circular gas injection at the flat plate into supersonic cross-flow by Santiago et al. [2]

The secondary injection into the supersonic convergent-divergent (C-D) nozzle has additional increase in complexity with interaction of the 3D nature, bounded main jet with the transverse secondary injection. Wall-effects and shock reflection are further affect 3D structures in the initiated flowfield. Thrust vectoring effects presented through the scope of forces acting on the nozzle maybe sorted as: 1. pressure forces acting on the nozzle wall, 2. viscous forces acting on the nozzle wall and 3. natural reactive force (momentum) of the secondary injection at the injection port. The main jet deflection is inducing force imbalance in lateral direction generating the force on the wall in direction opposite to the deflection. The general lateral or vector force is further increased with the dynalpy-flux or natural reactive force of the secondary jet.

In the current investigations two conical nozzles with the identical divergent sections and the two different second injection positions are investigated in the experiments, $x_j/x_t=0.7$ and $x_j/x_t=0.9$. With the aim to test system without additional pumps and with low-moderate mass-flow ratio, SPR is ranging up to unity value, while the secondary to primary mass-flow ratio is varying around 5%. Additionally to these experiments, numerical simulation on the same test models are performed in order to compare the results and to obtain relations between the input values and the resulting vectoring capabilities. Using the method of characteristics truncated ideal contour (TIC) nozzle of the same pressure ratios is designed, then corrected and numerically tested for SVC. As the analytical factor for comparing thrust vectoring capabilities, pitch thrust vector angle (δ) is selected that is defined as an arctangent ratio of normal and axial forces acting onto nozzle:

$$\delta = \arctan\left(\frac{F_v}{F_a}\right) \tag{2}$$

To make thrust vectoring evaluation relevant the above value needs to be paired with NPR, SPR and mass-flow ratio defined as: $f_m=(m_j/m_i)$.

2. Experimental setup

The experiments are performed at the Institute ICARE “FAST” platform using the super/hypersonic wind tunnel EDITH. The wind-tunnel is arranged, equipped and setup by the authors. The EDITH is set as the blow-down

type of the wind tunnel where clean, oil-free air is first dried, compressed till 300bars and stored in 320l tank. The air is supplied with 8mm tube to the pressure-regulator and after regulation through the 12mm diameter tube to the flow-splitter. From there, with 6 radial distributed 8mm tubes is injected to the settling chamber of 160mm diameter and exhausted in the test-section through the nozzle. The model of the engine is with lower chamber pressure of 3bars exhausting in the depressurized test section of a 0.08bar thus, simulating the conditions for the upper-stages of the launcher. The primary experiments are conducted with the 2 same conical type of the C-D axisymmetric nozzles of designed nozzle pressure ratios *NPR = 37,5*, throat radius of *9,72mm* and expansion ratio *Ath/Ae = 0.236* and the divergent conical half-angle of *5.42deg*. The circular *Dj=6mm* diameter injection port is normal to the nozzle axis and at $x_j/x_t=0.7$ for the first and at $x_j/x_t=0.9$ for the second conical nozzle. The secondary air is supplied through the 4 radial distributed tubes into the injectant settling chamber and from there smoothly via the convergent section to the sonic throat, Figure 4.
The implemented diagnostic tools are measuring the flow properties; the stagnation pressure and temperature in the main and secondary settling chambers, the ambient pressure and the temperature at the test section. The second nozzle is equipped with a Kulite parietal pressure transducer placed in the line with injection port at $x/x_t=0.35$. Flow visualization is obtained using the Toepler's Z-schlieren configuration at the exit of the nozzle, Figure 6a and 7a.
To measure forces, two-frame-complex balance is constructed using the HBM force transducers to measure the vertical, axial and lateral forces. All the diagnostic data is recorded using the "NI" SCXI DAQ acquisition cards and the LabView software package. The results are gathered and further treated using the designed programs in Matlab.

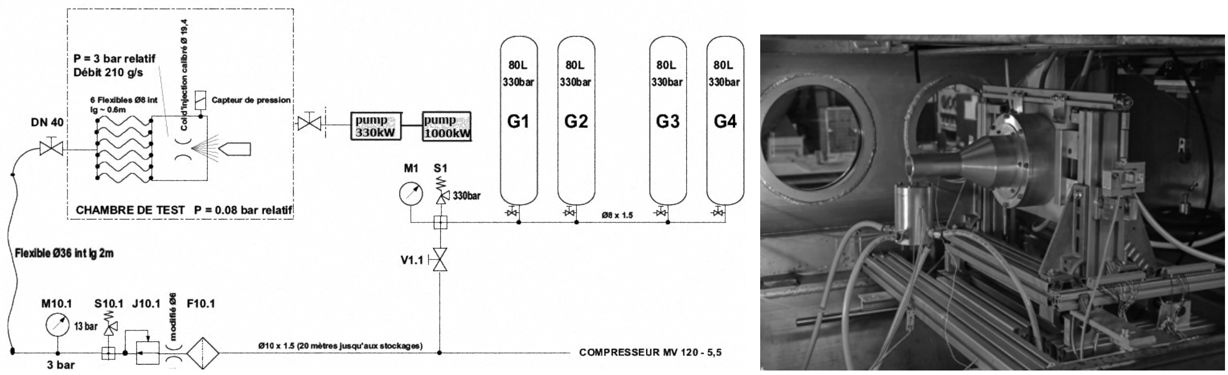

Figure 4: a) Scheme of the wind-tunnel operation b) Test engine system mounted on the balance

The experiments are performed keeping the adapted conditions for the nozzle of 3bars stagnation and 0,08bars ambient pressure. The flow was not preheated so the temperature was in constant descent from 260K to 243K. The second pressure was altered from 2 to 3,5bar with 0,5bar step and the test time was between 2 and 3 minutes.

3. Numerical models and simulation

Numerical simulations are performed with the CPS (Code pour la Propulsion Spatiale) which is developed by the CNES and Bertin [8] . The CPS is a three dimensional finite volume CFD code designed for the space propulsive flows, aimed to gather in this unified code all the numerical and physical properties required for CFD solutions of liquid and rocket engine flows. The mathematical model is based on the mass averaged Navier-Stokes equations written for compressible multi-species reacting flows with a fully accounted viscous effects. It is solving on the unstructured 3D computational grid. Time splitting is used for both explicit and implicit schemes of order up to 4 in time and up to 3 in space. For the multi-specie fluxes are computed on the cell interfaces with a Tuomi and HLLC (by Toro) schemes for ideal gases and HLLC (by Baten), AUSM+up, AUSM U, Euler for the real gases, Roe scheme is available for single specie computations. For the presented study Launder-Jones k-epsilon model with realisability viscous-damping function is used with strong coupling of the wall function and the turbulence model. Dry air with gamma(T) and Cp(T) as a 7th degree polynomials is used as the primary and secondary gas and with the same stagnation properties as the experimental setup. Flux vectors are evaluated at each time step using the 2nd order HLLC or Roe's upwind difference splitting. Integration is achieved with fully explicit solver setting time-step control from unsteady for highest time-accuracy to the steady optimized time step with CFL up to 0,3.

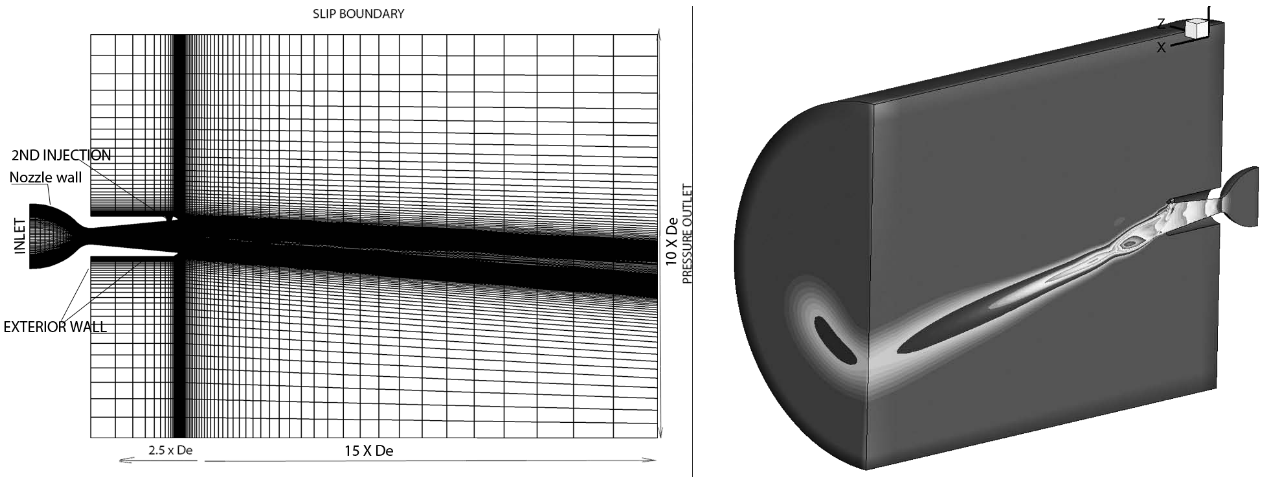

Figure 5: a) Computational grid b) 3D numerical domain with Mach number plot

The 3D computational grid is built on the test nozzle and exterior domain with the 1 million of mapped hexagonal elements. Nozzle domain consists of ~600000 hex-elements while the exterior domain has ~400000 hex elements, Figure 5a. Symmetry plane of the divergent section nozzle meshed with quadratic elements has 90 vertices in the normal and 210 vertices in the axial direction with graduation toward the throat and the secondary injection port. Exterior domain is 15 nozzle exit diameters in the downstream direction, 2.5 diameters in the upstream direction and 9 exit diameters in the radial direction. Boundary layer consists of 20 cells and 15 transitional cells with growth factor 1,14 and it is swept from throat towards the exit with first cell depth of 0.012mm at the throat section and 0.028 at the exit section. The y+ value is ranging in flow direction from 4 to 12.

To design the truncated ideal contour (TIC) nozzle, code based on modified method of characteristics is built with potential velocity as the marching characteristic and the Sauer's method for calculation of the sonic line as the initial condition, [15]. After the inviscid calculation and selection of the nozzle profile, several turbulence models, that are available in CPS, are used to test and correct preliminary nozzle profile for the boundary-layer.

The TIC nozzle is numerically investigated for 2 injector configurations, rectangular-slot and circular injection, and with several injection port position and angles. The width (*b*) of the slot injection is constructed in correlation with selected central angle of the arc on the nozzle wall and with centre on the nozzle axis, Figure 6. In the present study slot from central angle of $\varphi=30deg$ is investigated as the reference case. This value of central arc angle is in the range of best performing cases reported by the Wing, Guiliano [7].

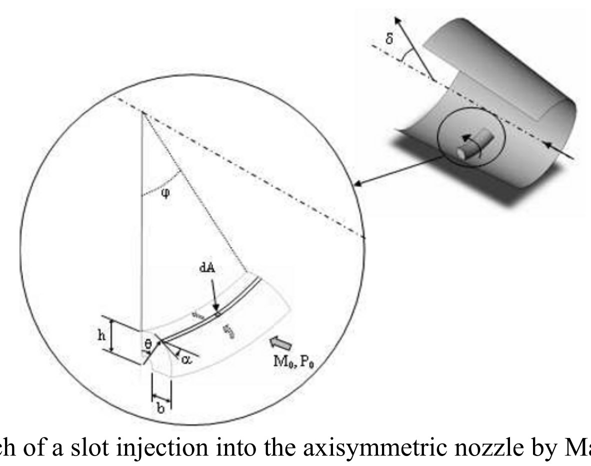

Figure 6: Sketch of a slot injection into the axisymmetric nozzle by Maarouf et al. [11]

4. Results

The numerical and experimental data of the two conical nozzles are compared in terms of force-balance measurements, pressures and flowfield schlieren visualization. Some previous analysis and numerical simulations showed that position of the injector closer to the nozzle exit increases TVC efficiency, as reported by Mangin [12]. The experiments and simulation with the preliminary nozzle with injector at $x_j/x_t = 0.7$ revealed the unwanted effects in the produced supersonic cross-flow, Figure 6.

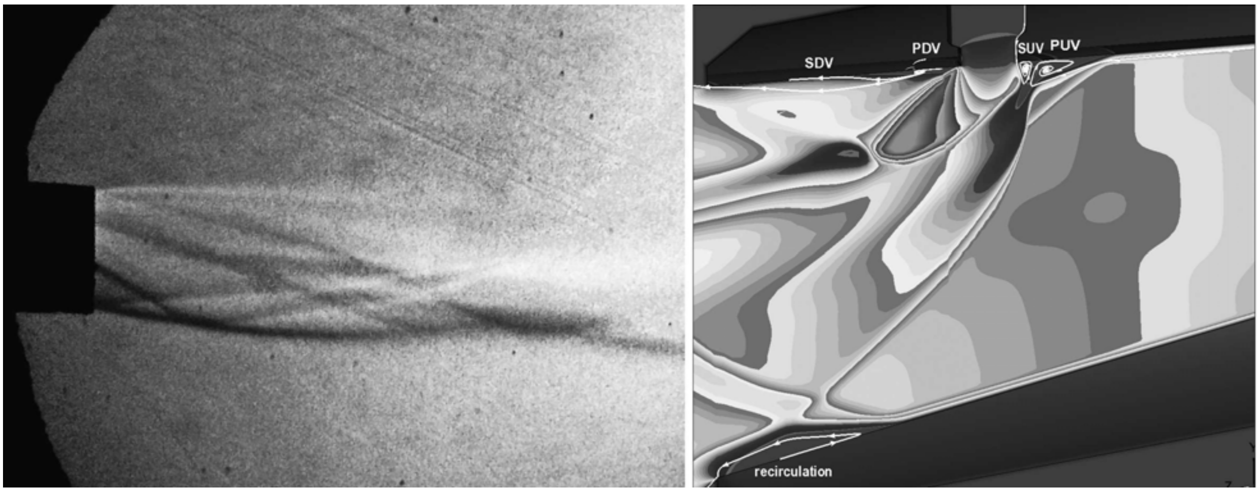

Figure 6: Nozzle a) Z-Schileren visualization b) 3D numerical flowfield

The leading-frontal surface of the bow-shock wave is reflecting from the opposite wall of the nozzle (Figure 6b), separating the BL and generating the recirculation zone, on the end lead to the negative vector side force on the wall. Downstream of the injector, the detached flow reattaches to the wall and with interaction of reflected shock it can lead to instabilities, also reported by Masuya et al.[6]

Injection closer to the nozzle exit $x_j/x_t = 0.9$ eliminates mentioned effects for the adapt-operated nozzle. The additional features of the nozzle flow are influencing vortex and flow structure of Santiago et al.[2] model as depicted on the Figure 7b. Lateral spread of the bow shock is restricted with the nozzle wall sides; the reflected side-end interacts with inner region pinching the 3D structures inside. In the conical nozzles usually present weak compression waves may additionally deform the structure. The effects occurring from the nozzle symmetry plane towards the lateral walls are superimposed on the Schlieren images which on some close regions give impression of double lines. Dimensionless wall pressure distribution Fig.8a gives the variation of the separation upstream and downstream of the injector, and single used parietal sensor matched numerical data. Force measurements presented versus the SPR and mass flow ratios in Table1 showed excellent matching with the numerical results.

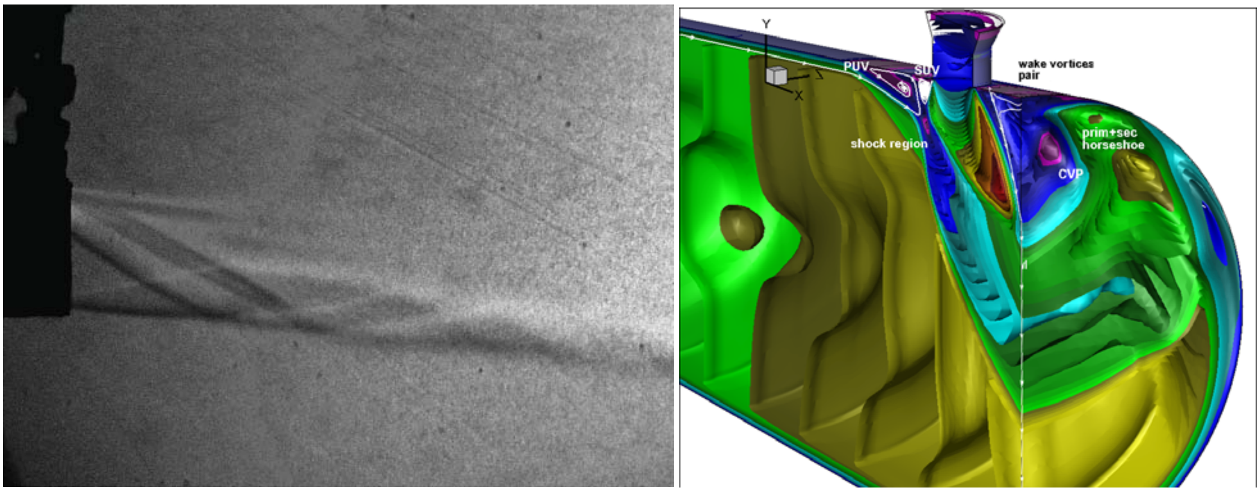

Figure 7: Nozzle $x_j/x_t=0.9$ a) Z-Schileren visualization b) 3D numerical flowfield

The value of the pitch vector angle δ can be speculative if not related with other values since decrease in thrust force will generate increase in ratio of normal to axial forces acting onto nozzle and thus increase of the fictive vectoring efficiency also. Therefore, the value of the NPR is kept in the design adapted regime of *NPR=37.5* while the SPR is varied. These results are presented in Table 1 with change of thrust specific impulse.

Table 1: Experimental and numerical result-data of flow properties and force measurements

SPR	f_m	$F_{jy[NUM]}$	$F_{wy[NUM]}$	F_v		F_a		δ		η
p_c/p_j	$\dot{m}_j / \dot{m}_i$	[N]	[N]	num	exp	num	exp	num	exp	I_{sv} / I_s
-	(223g/s)	-	-	-		126.38N	126.2N	-		(57.77s)
				Case 1: $x_j/x_t = 0.7$						
1	0.081	9.43	-5.86	3.572	4.60	130.31	131.05	1.57°	2.0°	0.954
				Case 2: $x_j/x_t = 0.9$						
0.667	0.055	6.63	6.04	12.67	12.4	127.76	126.8	5.67°	5.6°	0.959
0.833	0.068	8.02	6.92	14.94	15.0	128.39	128.3	6.64°	6.7°	0.951
1	0.081	9.88	8.3	18.18	18.4	128.5	127.8	8.05°	8.2°	0.942
1.167	0.098	11.47	9.30	20.77	20.5	128.89	127.3	9.15°	9.2°	0.927

The side-force value is gradually evolving with the increase of SPR which is directly proportional to the mass flow ratio that represents the most influential parameter for side vector force. At the figure 5b which depicts vectoring versus mass-flow ratio, optimal angle is found in the range of SPR=1 delivering the δ of 8.2^o for $m_j/m_i = 0.08$

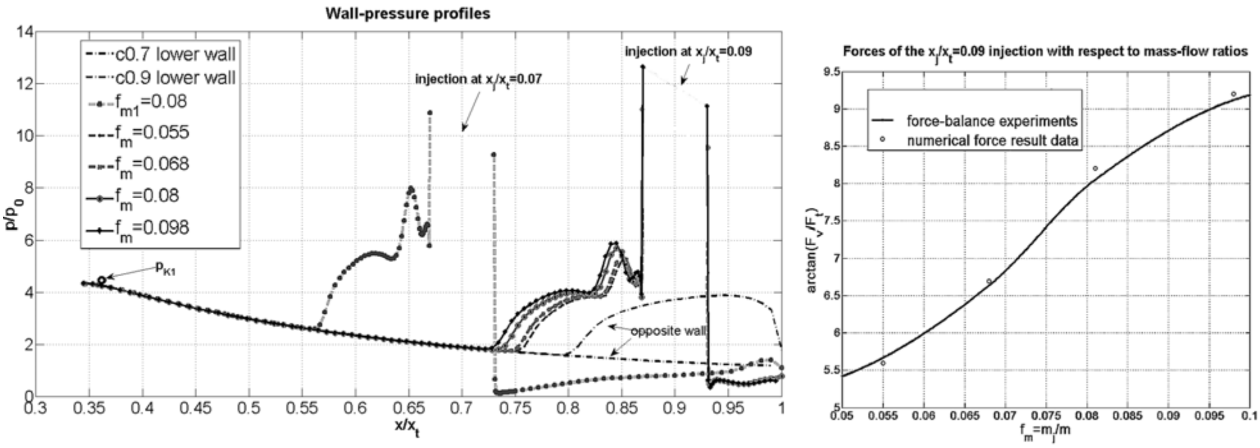

Figure 8: a) Dimensionless wall-pressure distribution b) δ – deflection angle versus f_m

The truncated ideal contour (TIC) nozzle of the same *NPR=37.5* and exit angle of 5.3^o is numerically tested. The simulations are performed with circular and slot injection at $x_j/x_t=0.9$ of the same area and thus the same injectant mass-flow rate. The slot was constructed with the central angle $\varphi=30^o$ which results in a sloth width of *b=2.7mm*.

In the case of slot injection larger amount of flow from the main jet is affected in the lateral direction resulting in separation position being placed further upstream and causing higher deflection force. The bow shock in this case is gaining somewhat smaller steep gradient from the injection plume since its penetration height is shorter, Figure 9b, but the lateral shock-front surface is quite larger which effectively deflects the main jet.

The circular injection with inclination from the nozzle axis has been investigated experimentally by Nielson et al. [1] and also by Masuya et al [10]. Nielson [1] performed experiments on series of the circular sonic injections of f_m~0.06 under different angles. It is found that downstream inclined injection has a negative effect on the side force while the upstream inclined angles positively affect the deflection until some limiting breakdown value of the angle in range of 130°.

On the Figure 9a the numerically obtained flowfield of the TIC nozzle with sonic circular upstream inclined injection is depicted. It can be observed that upstream boundary-layer detachment and separation region are being further displaced by the plume injected under angle towards the separation point which additionally pushes away detached flow. The generated bow shock therefore propagates steeper in the main jet and thus augmenting the side force.

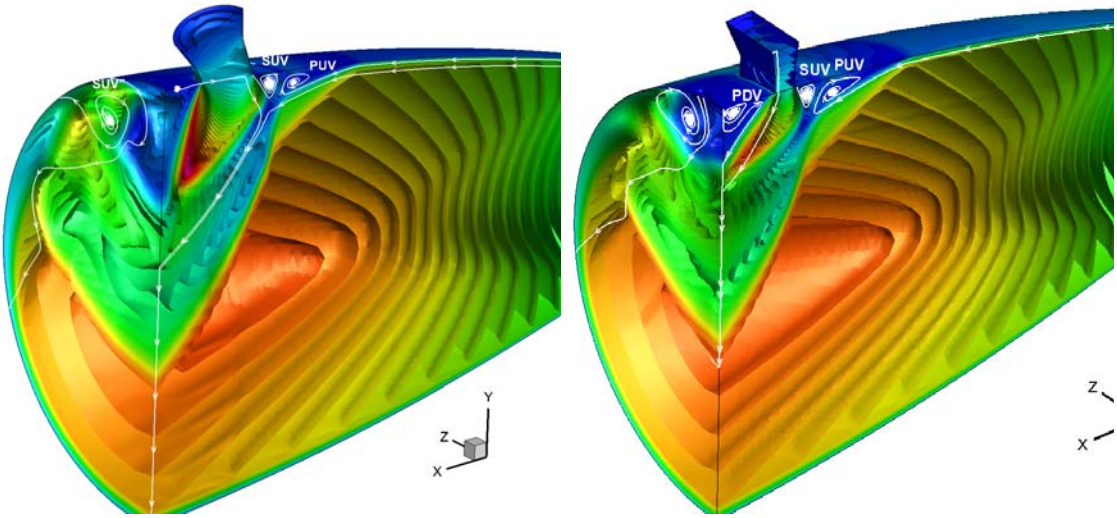

Figure 9: a) Circular injection with 110deg inclination upstream of the nozzle axis b) Slot injection normal to axis

Table 2: Numerical result-data of flow properties and force measurements of TIC nozzle for *SPR=1*, f_m*=0.08*

Injection case	$\boldsymbol{\theta}$ [°]	F_{jy} [N]	F_{wy} [N]	F_v $F_{jy}+F_{wy}$	F_a [N]	δ [°]	η I_{svx}/I_{sv}
Circular injection	90	10.03	7.41	17.44	136.5	7.28	0.94
Circular injection	110	10.07	9.57	19.64	134.95	8.28	0.93
Circular injection	120	10	10.36	20.36	134.06	8.64	0.92
Slot injection	90	9.86	8.96	18.82	137.01	7.82	0.94

On the diagram on Figure 10, dimensionless wall pressure distribution of the normal, inclined circular and normal slot sonic injection are given. Circular upstream inclined injection and slot injection cases separation point is noticeably further upstream displaced which affects the size of vortex and shock zones and thus the side force. As a consequence of wide, lateral injection in the slot case the first detachment region with PUV is noticeably larger developing from the point of detachment to the approximately same place as circular normal injection. At the circular injection under angle, first detachment zone is of the same size while the pick region and third region before injection are noticeably larger and responsible for separation point displacement. This leads to the assumption that optimal injection geometry should be investigated between the slot and the upstream angular injection.

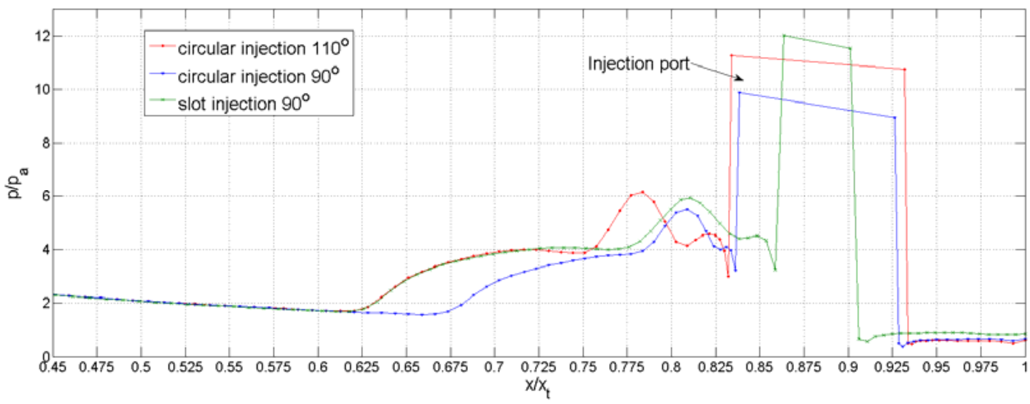

Figure 10: Wall-pressure distribution of normal, inclined circular and normal slot injection

Conclusions

Presented study of the thrust SVC for C-D axisymmetric nozzles showed that significant vector side force and pitch thrust-vector angle is possible to achieve. It has also revealed the influencing parameters and properties which should be investigated in the optimization process. The future steps in the ongoing study will be to experimentally and numerically investigate and optimize thrust SVC possibilities between more injector position, angles and injector shapes of the truncated ideal(TIC) and thrust optimized(TOC) contour nozzles. The investigations are being improved with the additional parietal and pressure taps, visualization techniques and higher numerical resolution. This will allow further improvement in the study and analysis of the possible low-frequency instabilities and different separation modes.

Acknowledgements

Special thanks to the French Space Agency (CNES) for collaboration and support and to the Mr. Gouillon N. for technical assistance in this study.

References

[1] Neilson J.H., Gilchrist A., Lee C.K. 1968. Side thrust control by secondary gas injection into rocket nozzles, *Journal Mechanical Engineering Science Vol. 10*, No.3, 239-251
[2] Santigo J.G., Dutton J. 1997. Crossflow vortices of a jet injected into a supersonic crossflow, *AIAA Journal Vol.35*, No.5, 915-917
[3] Spaid F.W., Zukoski E.E. 1968. Study of the interaction of gaseous jets from transverse slots with supersonic external flows, *AIAA Journal Vol.6*, No.2, 205-212
[4] Zukoski E.E. 1967. Turbulent boundary-layer separation in front of a forward-facing step, *AIAA Journal Vol.5* No.10, 1746-1753
[5] Guhse R.D. 1966. On secondary gas injections into supersonic nozzles, *AIAA Journal Vol.3* No.1, 147-149
[6] Schetz F.W., Billig E.E. 1966. Penetration of gaseous jets injected into a supersonic stream, *AIAA Journal Vol.3*, No.11, 1658-1665
[7] Avduevskii V.S., Medvedev K.I. Polyanskii M.N. 1970. Interaction of a supersonic flow with a transverse jet injected through a circular aperture in a plate, *Izvestiya Akademii Nauk SSSR, Mekhanika Zhidkosti i Gaza No.5*, 193-197
[8] Durand P., Vieille B, Lambare H, Vuillermoz P, Boure G, Steinfeld P, Godfroy F, Guery J.F. 2000. CPS: A three-dimensional CFD numerical code dedicated to space propulsive flows, *AIAA A00-36976 3864*
[9] Wing D.J., Giuliano V.J. 1997. Fluidic thrust vectoring of an axisymmetric exhaust nozzle at static conditions, *ASME FEDSM97-3228*
[10] Masuya G., Chinzei N., Ishii S. 1977. Secondary gas injection into a supersonic conical nozzle, *AIAA Journal 15, 3*
[11] Maarouf N., Sellam M., Grignon M., Chpoun A. 2007. Thrust vectoring through fluid injection in an axisymmetrical supersonic nozzle*, ISSW26 2*, 1141-1147
[12] Mangin B., Chpoun A., Jacquin L. 2006. Experimental and numerical study of the fluidic thrust vectoring of a two-dimensional supersonic nozzle, *AIAA 2006-3666*
[13] Erdem E., Kontis K. 2010. Numerical and experimental investigation of transverse injection flows, *Springer Shock Waves, 20,* 103-118
[14] Dussauge J.-P. 2009. Compressible turbulence in interaction of supersonic flows, *Springer Turbulence and Interactions NNFM 105*, 35-54
[15] Zucrow M., Hoffman J.D. 1977. Gas dynamics, *Willey and sons*
[16] Maarouf N. 2008. Modelling study of dissymmetrical phenomena in the divergent of supersonic propulsion nozzles : application to the thrust vectoring (en Français), thesis dissertation, December 2008